Dynamics of a Tethered Satellite Subjected to Aerodynamic Forces

Guido de Matteis* and Luciano M. de Socio†
University of Rome "La Sapienza," Rome, 00184 Italy

The equations of motion of a subsatellite and its tether are studied to show the influence of the aerodynamic forces on the equilibrium states of the system and the corresponding perturbed motion. It is shown that aerodynamic forces can play a major role in determining the stability of the system equilibrium states in situations of practical interest.

Nomenclature

A = tether cross section
a = tether diameter
c = damping coefficient
C_D = drag coefficient of subsatellite
C_d = drag coefficient of tether
C_x, C_y = aerodynamic force coefficients, Eq. (13)
E = Young's modulus
l = tether length
l_0 = tether length at zero tension, reference length
M = subsatellite mass
m = tether mass per unit length
n = real part of an eigenvalue
R_B = orbital radius of Shuttle
R_E = Earth radius
S = subsatellite reference area
s = curvilinear coordinate along the tether, Eq. (3)
t = time
u, v = velocity components
V = velocity modulus, Eq. (10)
X, Y = aerodynamic force components, Eqs. (8-9)
x, y = coordinates
ϵ = stretching, Eq. (18)
Π = gravitational constant
ρ = atmospheric density, Eq. (12)
ρ_1 = atmospheric density at sea level: reference density
τ = tether tension, Eq. (4)
ϕ = imaginary part of an eigenvalue
ω = orbital velocity of the Shuttle, Eq. (11): ω^{-1} is the reference time
Ω = Earth angular velocity

Subscripts

B = at $s = 0$
e = steady state
l = at $s = l$
0 = unstretched

Superscripts

$'$ = perturbation variables
$\sim$ = dimensionless variables

Received Dec. 14, 1989; presented as Paper 90-0656 at the AIAA 28th Aerospace Sciences Meeting, Reno, NV, Jan. 8-11, 1990; revision received May 7, 1990; accepted for publication May 14, 1990. Copyright © 1990 by the American Institute of Aeronautics and Astronautics, Inc. All rights reserved.

*Research Scientist, Department of Mechanics and Aeronautics, via Eudossiana 18. Member AIAA.

†Professor, Department of Mechanics and Aeronautics, via Eudossiana 18.

I. Introduction

THE dynamics of a tethered satellite deployed from an orbiting Shuttle has been investigated in a rather large number of papers. All of these articles can be grouped into categories according to the various research objectives that have appeared at an increasing rate as the time of the first mission grows shorter. Reference is made here to the collection of results presented at dedicated meetings[1-3] and to articles on the subject which appeared in technical journals. Some gray areas still remain in the corpus of works, and this happened each time it was felt that the details of some peculiar question could be delayed to less cogent times, since these details appeared to be of a minor practical importance.

A careful inspection of the literature concerning the dynamics of tethered satellites shows that consideration has been given to the study of the effects of the aerodynamic forces and moments on the subsatellite and the tether, in connection with applications of the subsatellite such as using it as an orbiting wind tunnel.[4] The aerodynamic forces are almost negligible compared with the inertial, gravity, and elastic forces in a large number of cases, but the review of Ref. 5 already indicates a number of situations where they can produce great effects on the stability of the system. This is the case where the oblateness of the Earth, the eccentricy, and the inclination of the orbit of the Shuttle are taken into account.

A few references[6,7] have already pointed out through a simple approach the interactions of the atmosphere with the subsatellite which lead to instability. Apart from the destiny of the tether-subsatellite system in an unstable situation, one should then be thoughtful of the Shuttle itself and of its safety.

In a recent paper,[8] the problem of the equilibrium and stabilty of the Shuttle-tether-subsatellite system is reconsidered in which the tether is massless and aerodynamic forces act on the subsatellite only. In Ref. 8, a stability criterion is provided and it is confirmed that instabilities can be caused by the atmospheric density gradient. This is an example of how small forces can produce unstable consequences through resonances involving aerodynamic, inertial, and elastic forces, and the orbital motion of the Shuttle.

Here, the inertia of the tether and the aerodynamic forces on it are included in the model, in order to determine the time history of the system and the stability conditions on an initial equilibrium or—better—on an initial steady state. From the mathematical point of view, in the present case, the problem is governed by a set of nonlinear, partial differential equations.

A number of assumptions are made to limit the complexity of a fully realistic model. In particular, thermal effects on the structures and on the aerodynamic coefficients, the effects of the oblateness of the Earth, the dynamic character of the atmosphere, the terrestrial magnetic field, and the peculiarities of the ionospheric layers through which part of the system can move are neglected. Furthermore, the Shuttle is considered to move on a circular orbit in the equatorial plane and use will be

made of the reduced gravity, i.e., of an approximate linear formula for the gravity gradient force,[9] in the equations of motion. Finally, we will assume that the atmosphere rotates with the same angular speed of the Earth and that the Shuttle proceeds at a constant angular velocity on its path.

Since the main goal of this paper is to achieve a better understanding of the dynamic behavior of the tethered subsatellite, attention will be mostly focused on the physically meaningful results, without entering too deeply into an extended description of the mathematical tools that have been used. In the first part of the work, the equations of motion are linearized about the equilibrium state and the stability of this steady condition is discussed. In the second part, the full set of nonlinear equations are solved in order to follow the time history of the system as influenced by its initial state and by the values of the characteristic parameters.

II. Basic Equations and Characteristic Products

A sketch of the system considered is shown in Fig. 1. To describe the motion of the system, we use a planar rotating Cartesian system that is centered in the mass center of the Shuttle, with the x axis pointing downward along the local vertical and the y axis opposite to the velocity on the circular orbit of radius R_B. Within the framework of hypotheses already discussed, the basic system of equations governing the motion of the subsatellite and of the cable is the one obtained in Ref. 10, with extension to an elastic tether.[11,12] We have

$$m(\dot{u}-2\omega v-3\omega^2 x)=\frac{\partial}{\partial s}\left(\tau\frac{\partial x}{\partial s}\right)+X \tag{1}$$

$$m(\dot{v}+2\omega u)=\frac{\partial}{\partial s}\left(\tau\frac{\partial y}{\partial s}\right)+Y \tag{2}$$

with $u=\dot{x}$ and $v=\dot{y}$.

The tension in the cable τ, at the curvilinear abscissa s given by

$$s=\int_0^{s_0}\left[\left(\frac{\partial x}{\partial s_0}\right)^2+\left(\frac{\partial y}{\partial s_0}\right)^2\right]^{1/2}d\eta \tag{3}$$

is

$$\tau=EA\left\{\left[\left(\frac{\partial x}{\partial s_0}\right)^2+\left(\frac{\partial y}{\partial s_0}\right)^2\right]^{1/2}-1\right\}+c\dot{s} \tag{4}$$

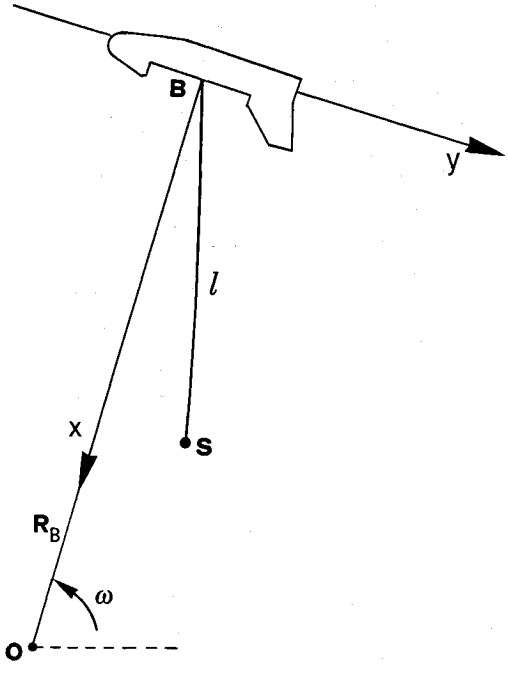

Fig. 1 Sketch of the tether-subsatellite system.

The boundary conditions at the attachment point B of the tether to the Shuttle are

$$x_B=x(s=0,t)=0, \qquad y_B=y(s=0,t)=0 \tag{5a}$$

$$u_B=u(s=0,t)=0, \qquad v_B=v(s=0,t)=0 \tag{5b}$$

whereas at the free end of the cable

$$M(\dot{u}_l-2\omega v_l-3\omega^2 x_l)=-\tau\left(\frac{\partial x}{\partial s}\right)_l+X_l \tag{6a}$$

$$M(\dot{v}_l+2\omega u_l)=-\tau\left(\frac{\partial y}{\partial s}\right)_l+Y_l \tag{6b}$$

where $u_l=u(s=l,t)$ and $v_l=v(s=l,t)$. The initial conditions are

$$x(s,t=0)=x_e(s), \qquad y(s,t=0)=y_e(s) \tag{7a}$$

$$u(s,t=0)=0, \qquad v(s,t=0)=0 \tag{7b}$$

The components of the aerodynamic forces are expressed as

$$X=-\tfrac{1}{2}\rho C_x aVu \tag{8}$$

$$Y=-\tfrac{1}{2}\rho C_y aV\left[v-\omega(R_B-x)(1-\Omega/\omega)\right] \tag{9}$$

and

$$X_l=-\tfrac{1}{2}\rho_l C_D SV_l u_l$$

$$Y_l=-\tfrac{1}{2}\rho_l C_D SV_l\left[v_l-\omega(R_B-x_l)(1-\Omega/\omega)\right]$$

The local velocity is given by

$$V=\left\{\left[v-\omega(R_B-x)(1-\Omega/\omega)\right]^2+u^2\right\}^{1/2} \tag{10}$$

and we have, for the orbital velocity and the density, respectively,

$$\omega=\left(\Pi/R_B^3\right)^{1/2} \tag{11}$$

$$\rho=\rho_1 f(R_B-R_E-x) \tag{12}$$

In this paper, the tabulated values of the Standard Atmosphere[13] will be used.

Following Ref. 10, the aerodynamic coefficients in Eqs. (8) and (9) will be taken as

$$C_x=0, \qquad C_y=C_d(\partial x/\partial s) \tag{13}$$

After a proper set of reference units is chosen, the dimensionless form of the governing Eqs. (1-12), with Eq. (13), is

$$\tilde{u}-2\tilde{v}-3\tilde{x}=\frac{\partial}{\partial\tilde{s}}\left[(\Pi_S\epsilon+\Pi_d\tilde{s})\frac{\partial\tilde{x}}{\partial\tilde{s}}\right] \tag{14}$$

$$\tilde{v}+2\tilde{u}=\frac{\partial}{\partial\tilde{s}}\left[(\Pi_S\epsilon+\Pi_d\tilde{s})\frac{\partial\tilde{y}}{\partial\tilde{s}}\right]+\tilde{Y} \tag{15}$$

where

$$\tilde{Y}=-\Pi_A\left(\frac{\partial\tilde{x}}{\partial\tilde{s}}\right)\tilde{\rho}\tilde{V}\left[\tilde{v}-\Pi_\omega(\Pi_l-\tilde{x})\right] \tag{16a}$$

$$\tilde{V}=\left\{\left[\tilde{v}-\Pi_\omega(\Pi_l-\tilde{x})\right]^2+\tilde{u}^2\right\}^{1/2} \tag{16b}$$

$$\tilde{\rho}=g\left[\Pi_l\left(1-\frac{1}{\Pi_R}\right)-\tilde{x}\right] \tag{16c}$$

and, at the free end,

$$\tilde{u}_l - 2\tilde{v}_l - 3\tilde{x}_l = -\Pi_M(\Pi_S \epsilon_l + \Pi_d \tilde{s}_l)\left(\frac{\partial \tilde{x}}{\partial \tilde{s}}\right)_l + \Pi_M \tilde{X}_l \quad (17a)$$

$$\tilde{v}_l + 2\tilde{u}_l = -\Pi_M(\Pi_S \epsilon_l + \Pi_d \tilde{s}_l)\left(\frac{\partial \tilde{y}}{\partial \tilde{s}}\right)_l + \Pi_M \tilde{Y}_l \quad (17b)$$

whereas the dimensionless form of the boundary condition at $\tilde{s}=0$ and of the initial conditions are obvious, and where

$$\tilde{X}_l = -\Pi_A \Pi_C \tilde{\rho}_l \tilde{V}_l \tilde{u}_l$$

$$\tilde{Y}_l = -\Pi_A \Pi_C \tilde{\rho}_l \tilde{V}_l [\tilde{v}_l - \Pi_\omega(\Pi_l - \tilde{x}_l)]$$

$$\tilde{s} = \int_0^{\tilde{s}_0} \left[\left(\frac{\partial \tilde{x}}{\partial \tilde{s}_0}\right)^2 + \left(\frac{\partial \tilde{y}}{\partial \tilde{s}_0}\right)^2\right]^{1/2} d\tilde{\eta}$$

The local stretching ϵ with respect to a tensionless state is

$$\epsilon = \left[\left(\frac{\partial \tilde{x}}{\partial \tilde{s}_0}\right)^2 + \left(\frac{\partial \tilde{y}}{\partial \tilde{s}_0}\right)^2\right]^{1/2} - 1 \quad (18)$$

The following set of characteristic products appears in the fundamental equations

$$\Pi_M = \frac{m l_0}{M}, \quad \Pi_S = \frac{EA}{m\omega^2 l_0^2}, \quad \Pi_R = \frac{R_B}{R_E}, \quad \Pi_l = \frac{R_B}{l_0}$$

$$\Pi_A = \frac{\rho_1 C_d a l_0}{2m}, \quad \Pi_C = \frac{C_D S}{C_d a l_0}, \quad \Pi_\omega = 1 - \frac{\Omega}{\omega}, \quad \Pi_d = \frac{c}{m l_0 \omega}$$

and Table 1 can help to get an idea of the practical ranges of the parameters on which the solution depends.

Since a full parametric investigation is out of the question, in the sequel one will only consider the influences of the variations of the dimensionless products due to changes of the length of the tether and of the mass of the subsatellite, keeping all of the remaining quantities constant and equal to reasonable values.

III. Equilibrium and Stability

For convenience, in what follows, the tilde will be dropped from the dimensionless quantities unless it is necessary to retain it for clarity. When the equilibrium conditions of the system are considered, the motion equations greatly simplify. In this steady situation, one has

$$3x_e + \Pi_S\left[\frac{\partial}{\partial s}\left(\epsilon \frac{\partial x}{\partial s}\right)\right]_e = 0 \quad (19)$$

$$\Pi_S\left[\frac{\partial}{\partial s}\left(\epsilon \frac{\partial y}{\partial s}\right)\right]_e + \Pi_A \Pi_\omega^2 \rho (\Pi_l - x_e)^2 \left(\frac{\partial x}{\partial s}\right)_e = 0 \quad (20)$$

with the boundary conditions at the free end

$$3x_{l_e} - \Pi_M \Pi_S\left[\epsilon_l \left(\frac{\partial x}{\partial s}\right)_l\right]_e = 0 \quad (21a)$$

$$\Pi_S\left[\epsilon_l \left(\frac{\partial y}{\partial s}\right)_l\right]_e - \Pi_A \Pi_C \Pi_\omega^2 \rho_l (\Pi_l - x_{l_e})^2 = 0 \quad (21b)$$

and

$$x_{B_e} = y_{B_e} = 0 \quad (22)$$

Our past experience has shown us that in some cases the sensitivity of the stability analysis to the solution of the equilibrium equations is great. A good deal of effort was therefore spent to get an excellent accuracy in solving the nonlinear boundary value problem [Eqs. (19-22)]. Good results were obtained[14] by applying a modified Bellman differential quadrature procedure[15] to the case of the equilibrium of an inextensible tether.

Table 1 Range of the characteristic products

Product	Range
Π_M	6×10^{-2}–3
Π_S	57–1.2×10^4
Π_R	1.03–1.04
Π_l	66–700
Π_A	1.3×10^3–1.3×10^4
Π_C	1.7×10^{-2}–1.7×10^{-1}
Π_ω	9.38×10^{-2}–9.58×10^{-2}
Π_d	1–30

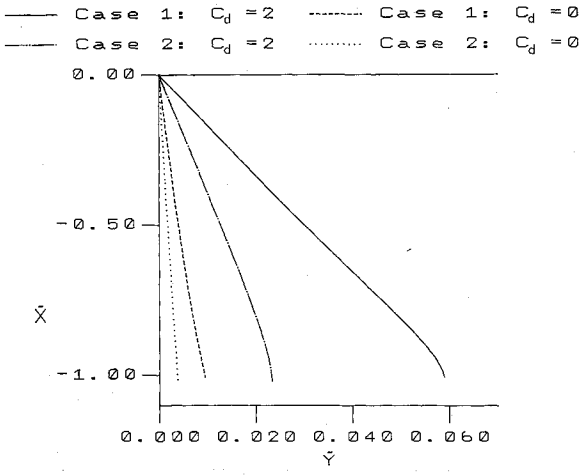

Fig. 2 Equilibrium solutions ($l_0=80$ km, $C_D=2$). Case 1: $M=250$ kg; and Case 2: $M=1000$ kg.

In the present circumstances, better approximations were obtained by a procedure first proposed by Satofuka.[16] As in the finite element method, a continuous approximation of the solution is assumed between the boundary points by means of a high-degree polynomial. The entire length of the cable is divided into $(N-1)$ parts by N nodes, and the space derivatives in each node are expressed by a combination of the values of the unknown variable in L adjacent nodes. The coefficients of such a combination are calculated by taking Lagrange-type polynomials as test functions.

A few significant equilibrium configurations are shown in Fig. 2 as functions of the dimensionless space coordinates, for two different values of the mass of the tethered subsatellite. In these cases, as for all of the results discussed in the following applications, it will be taken $R_B - R_E = 200$ km, $E=7\times10^{10}$ N/m^2, $a=6\times10^{-4}$ m, $m=5.76\times10^{-3}$ kg/m.

In each case, the effects of the aerodynamic forces acting on the cable are evident as expected. They decrease with an increase in the weight of the subsatellite. The distributed mass of the tether and the aerodynamic forces on it have contrasting effects on the curvature of the cable.

Let $\Xi=(x,y,u,v)$ be the state variable of the system. We now proceed to the linearization of the equations in the case of small perturbations $\Xi'=(x',y',u',v')$ about the initial equilibrium $\Xi_e=(x_e,y_e,0,0)$, namely

$$\Xi = \Xi_e + \Xi'$$

Two equations of the linearized set are the kinematic relations $\dot{x}'=u'$, and $\dot{y}'=v'$; and the rest of the system is given in Table 2, together with the boundary conditions at the free end.

With reference to the discrete model of the cable which has been already considered for evaluating the solution at equilibrium, the set obtained from the equations in Table 2, after introducing the linear combinations of the values of the un-

Table 2 Linearized equations of motion

$$\dot{u}' = 2v' + 3x' + \Pi_S \frac{\partial}{\partial s}\left\{\left[\epsilon + \left(\frac{\partial x}{\partial s}\right)^2\right]_e \frac{\partial x'}{\partial s} + \left(\frac{\partial x \partial y}{\partial s^2}\right)_e \frac{\partial y'}{\partial s}\right\} - \Pi_S\left[\frac{\partial}{\partial s}\left(\epsilon \frac{\partial x}{\partial s}\right)\right]_e$$
$$\times\left[\left(\frac{\partial x}{\partial s}\right)_e \frac{\partial x'}{\partial s} + \left(\frac{\partial y}{\partial s}\right)_e \frac{\partial y'}{\partial s}\right] + \Pi_d\left[\left(\frac{\partial^2 x}{\partial s^2}\right)_e \int_0^{s_0} (1+\epsilon_e)h'\,d\eta + \left(\frac{\partial x}{\partial s}\right)_e h'\right]$$

$$\dot{v}' = -2u' + \Pi_S \frac{\partial}{\partial s}\left\{\left(\frac{\partial x \partial y}{\partial s^2}\right)_e \frac{\partial x'}{\partial s} + \left[\epsilon + \left(\frac{\partial y}{\partial s}\right)^2\right]_e \frac{\partial y'}{\partial s}\right\} - \Pi_S\left[\frac{\partial}{\partial s}\left(\epsilon \frac{\partial y}{\partial s}\right)\right]_e$$
$$\times\left[\left(\frac{\partial x}{\partial s}\right)_e \frac{\partial x'}{\partial s} + \left(\frac{\partial y}{\partial s}\right)_e \frac{\partial y'}{\partial s}\right] + \Pi_d\left[\left(\frac{\partial^2 y}{\partial s^2}\right)_e \int_0^{s_0} (1+\epsilon_e)h'\,d\eta + \left(\frac{\partial y}{\partial s}\right)_e h'\right] + Y'$$

$$Y' = -2\Pi_A \Pi_\omega \rho_e (\Pi_l - x_e)\left\{\left(\frac{\partial x}{\partial s}\right)_e v' - \Pi_\omega\left[\frac{1}{2}(\Pi_l - x_e)\left(\frac{1}{\rho}\frac{\partial \rho}{\partial x}\right)_e - 1\right]\left(\frac{\partial x}{\partial s}\right)_e x' - \frac{1}{2}\Pi_\omega(\Pi_l - x_e)\right.$$
$$\left.\times\left[\left(\frac{\partial y}{\partial s}\right)_e^2 \frac{\partial x'}{\partial s} - \left(\frac{\partial x \partial y}{\partial s^2}\right)_e \frac{\partial y'}{\partial s}\right]\right\}$$

$$h' = \left(\frac{\partial x}{\partial s}\right)_e \frac{\partial u'}{\partial s} + \left(\frac{\partial y}{\partial s}\right)_e \frac{\partial v'}{\partial s}$$

Boundary conditions at the free end

$$\dot{u}_l' = 2v_l' + 3x_l' - \Pi_M \Pi_S\left\{\left[\epsilon_l + \left(\frac{\partial x}{\partial s}\right)_l^2\right]_e \left(\frac{\partial x'}{\partial s}\right)_l + \left[\left(\frac{\partial x \partial y}{\partial s^2}\right)_l\right]_e \left(\frac{\partial y'}{\partial s}\right)_l\right\}$$
$$- \Pi_A \Pi_C \Pi_M \Pi_\omega\left[\rho(\Pi_l - x_l)\right]_e u_l' - \Pi_M \Pi_d\left[\left(\frac{\partial x}{\partial s}\right)_l\right]_e \int_0^{s_0} (1+\epsilon_{l_e})h_l'\,d\eta$$

$$\dot{v}_l' = -2u_l' - \Pi_M \Pi_S\left\{\left[\left(\frac{\partial x \partial y}{\partial s^2}\right)_l\right]_e \left(\frac{\partial x'}{\partial s}\right)_l + \left[\epsilon_l + \left(\frac{\partial y}{\partial s}\right)_l^2\right]_e \left(\frac{\partial y'}{\partial s}\right)_l\right\} - 2\Pi_A \Pi_C \Pi_M \Pi_\omega\left[\rho(\Pi_l - x_l)\right]_e$$
$$\times\left\{v_l' - \Pi_\omega\left[\frac{1}{2}(\Pi_l - x_l)\left(\frac{1}{\rho}\frac{\partial \rho}{\partial x}\right)_l - 1\right]_e x_l'\right\} - \Pi_M \Pi_d\left[\left(\frac{\partial y}{\partial s}\right)_l\right]_e \int_0^{s_0} (1+\epsilon_{l_e})h_l'\,d\eta$$

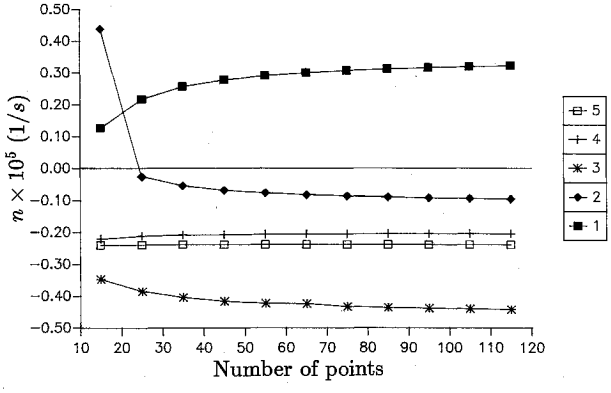

Fig. 3 Effect of the discretization on the stability analysis ($l_0 = 80$ km, $M = 1000$ kg).

knowns in the nodes and taking into account the boundary conditions, provides a system of $4(N-1)$ homogeneous ordinary differential equations for the unknowns in the nodes. This system can be put in the form

$$\dot{\xi} = A\xi \tag{23}$$

where

$$\xi^T = (x_i', y_i', u_i', v_i'), \qquad i = 1, \ldots, N-1 \tag{24}$$

The computation of the eigenvalues and of the eigenvectors of matrix A, whose elements are $[4(N-1)]^2$, is then matter of routine. Note that the elements of A contain the results of the evaluation of the state of the system in equilibrium together with the coefficients of the expansion of the derivatives according to Ref. 16.

Following the guidelines indicated above, the stability of the equilibrium was investigated. A relatively simple criterion cannot be established in the present situation as it was possible in the case of no aerodynamic forces on a massless tether.[8]

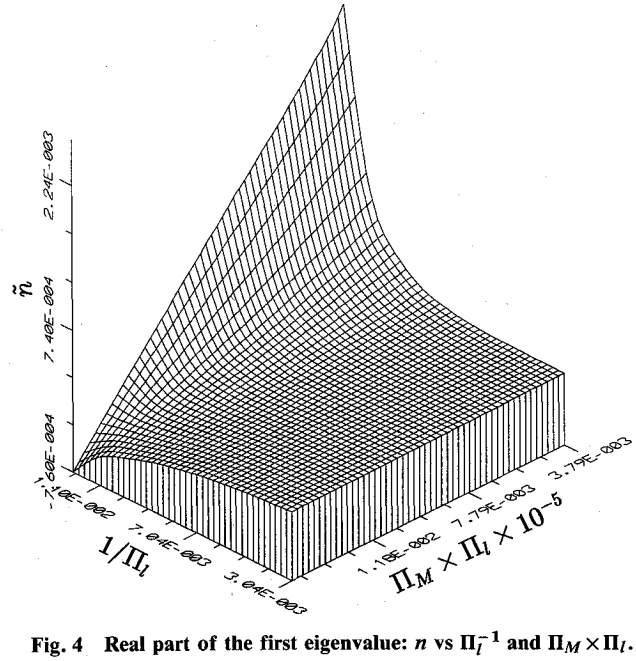

Fig. 4 Real part of the first eigenvalue: n vs Π_l^{-1} and $\Pi_M \times \Pi_l$.

Figure 3 shows the influence of the number of nodes N on the computational process. In particular, Fig. 3 reports the real parts of the eigenvalues $(n + i\phi)$ in an unstable situation, for the first five modes. As it will be seen later, the third mode corresponds to a predominantly longitudinal elastic oscillation, whereas the second, the fourth, and the fifth modes are predominantly transverse vibrations. The coefficients of the imaginary part show much faster convergence characteristics than the real part and are almost independent of N. The num-

ber of elements to reach a satisfactory convergence increases as l_0 increases and M decreases. In all of the calculations, the results of which are reported here, N could be as high as 115 and L, the number of adjacent nodes, equal either to 3 or to 5, the values depending on the required accuracy.

Figure 4 shows the values of the real part of the first eigenvalue as functions of two basic dimensionless parameters, namely, Π_l^{-1} and $\Pi_M \times \Pi_l$, all positive values corresponding, of course, to unstable equilibria.

A better interpretation of the results can be obtained by inspection of Fig. 5, where the iso-n lines are depicted in the plane $(\Pi_l^{-1}) - (\Pi_M \times \Pi_l)$. Since these two dimensionless groups correspond to l_0/R_B and to mR_B/M, respectively, the representation in Fig. 5 gives a rather direct answer about the effects of the length of the cable and of the mass of the suspended satellite. Clearly the limit line for stability is for $n = 0$. As a general fact, the first eigenvalue to have a positive real part is the one corresponding to the first mode (pendular mode). In all of the cases, only the pendular mode was observed to go unstable and no instance of aeroelastic instabilities was detected.

A comparison of the effectiveness of various models adopted for describing the stability characteristics of a tethered satellite system can be carried out by inspecting Fig. 6, where dimensional units are used to provide a better feeling of the entities involved. Case 1 is relative to a model where the mass of the cable and the aerodynamic forces on it are neglected.[8] Case 2 refers to a model that takes into account the mass of the tether but neglects the aerodynamic forces. Case 3 corresponds to the model that is investigated here. Figures 6a and 6b are for two different lengths of the cable, all other physical quantities being kept constant. The very significant role that is played by the aerodynamic forces on the tether should be noted. These forces cause instability in circumstances where the other two models predict stability. Care should be paid when comparing case 1 to cases 2 and 3 since the total mass of the system changes from M to $(M + ml_0)$.

An interesting, approximate method for the evaluation of the eigenfunctions, dealing with a model where all of the aerodynamic forces are neglected, is proposed in Ref. 17. However, in that reference there is a sample case, carried out numerically, which corresponds to an assumed initial equilibrium situation that in reality is unstable according to what has been said before.

When dealing with the calculated eigenvalues, some further meaningful results are given in Table 3 where, again, the values

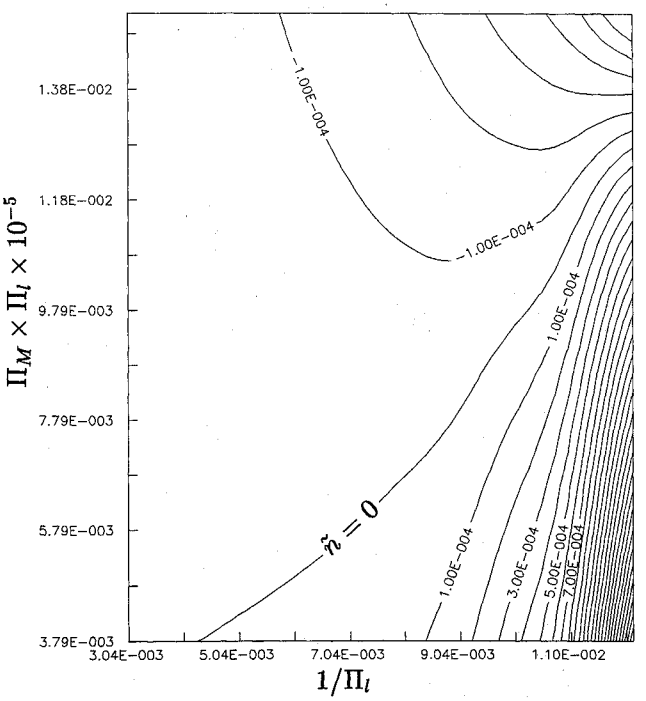

Fig. 5 Iso-n lines.

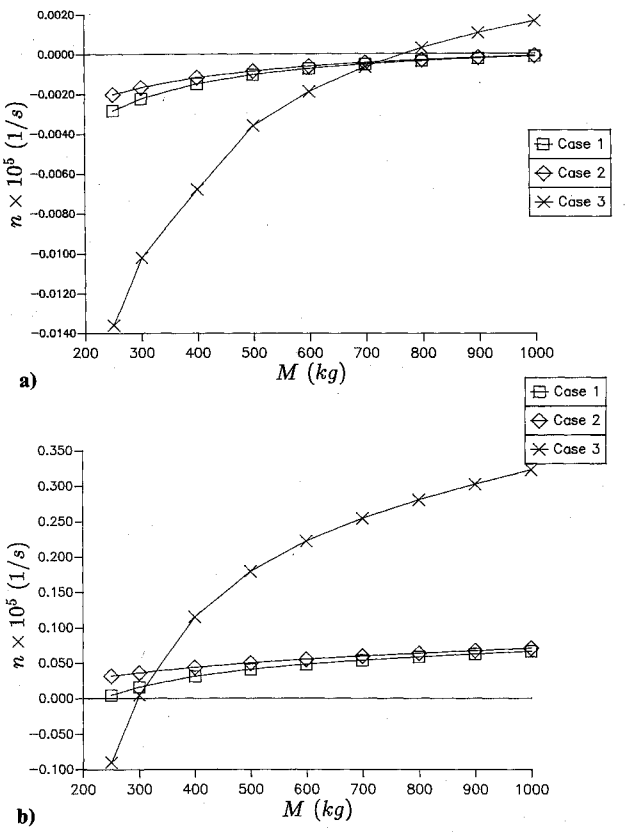

Fig. 6 Effect of the model on the stability analysis ($C_D = 2$): a) $l_0 = 40$ km; and b) $l = 80$ km. Case 1: $m = 0$, $C_d = 0$; Case 2: $m = 5.8 \times 10^{-3}$ kg/m, $C_d = 0$; and Case 3: $m = 5.8 \times 10^{-3}$ kg/m, $C_d = 2$.

Table 3 Effect of cable damping on stability

l_0, km	M, kg	c, kg/s	Eigenvectors 1st mode	Eigenvectors 1st longitudinal mode
80	1000	0	$3.22 \times 10^{-6} \pm 2.03 \times 10^{-3} i$	$-4.43 \times 10^{-6} \pm 1.47 \times 10^{-2} i$
		2	$2.99 \times 10^{-6} \pm 2.03 \times 10^{-3} i$	$-4.27 \times 10^{-4} \pm 1.46 \times 10^{-2} i$
80	250	0	$-8.99 \times 10^{-7} \pm 2.08 \times 10^{-3} i$	$-1.51 \times 10^{-6} \pm 2.35 \times 10^{-2} i$
		2	$-1.26 \times 10^{-6} \pm 2.08 \times 10^{-3} i$	$-2.32 \times 10^{-3} \pm 2.37 \times 10^{-2} i$
40	1000	0	$1.68 \times 10^{-8} \pm 2.04 \times 10^{-3} i$	$-7.80 \times 10^{-8} \pm 2.15 \times 10^{-2} i$
		2	$-3.57 \times 10^{-8} \pm 2.04 \times 10^{-3} i$	$-4.63 \times 10^{-4} \pm 2.15 \times 10^{-2} i$
40	250	0	$-1.30 \times 10^{-7} \pm 2.05 \times 10^{-3} i$	$-9.32 \times 10^{-8} \pm 3.88 \times 10^{-2} i$
		2	$-1.49 \times 10^{-7} \pm 2.05 \times 10^{-3} i$	$-1.49 \times 10^{-3} \pm 3.87 \times 10^{-2} i$

Table 4 Eigenvector components at the end point of the first three modes

Mode no.	$1(\tilde{\phi}=1.77)$	$2(\tilde{\phi}=8.40)$	$3(\tilde{\phi}=11.50)$
$C_d=0$ $\tilde{x}_{l_r}$	$2.3\times10^{-3}\pm9.6\times10^{-9}i$	$1.4\times10^{-5}\pm1.4\times10^{-8}i$	$0\pm1.4\times10^{-2}i$
$C_D=0$ $\tilde{y}_{l_r}$	$0\pm8.5\times10^{-2}i$	$3.7\times10^{-9}\pm2.6\times10^{-3}i$	$2.4\times10^{-3}\pm1.5\times10^{-9}i$
$C_d=2$ $\tilde{x}_{l_r}$	$2.3\times10^{-3}\pm5.8\times10^{-3}i$	$1.7\times10^{-5}\pm7.5\times10^{-3}i$	$-2.6\times10^{-5}\pm1.4\times10^{-2}i$
$C_D=2$ $\tilde{y}_{l_r}$	$8.4\times10^{-4}\pm8.3\times10^{-2}i$	$-2.5\times10^{-4}\pm2.7\times10^{-3}i$	$2.5\times10^{-3}\pm5.9\times10^{-4}i$

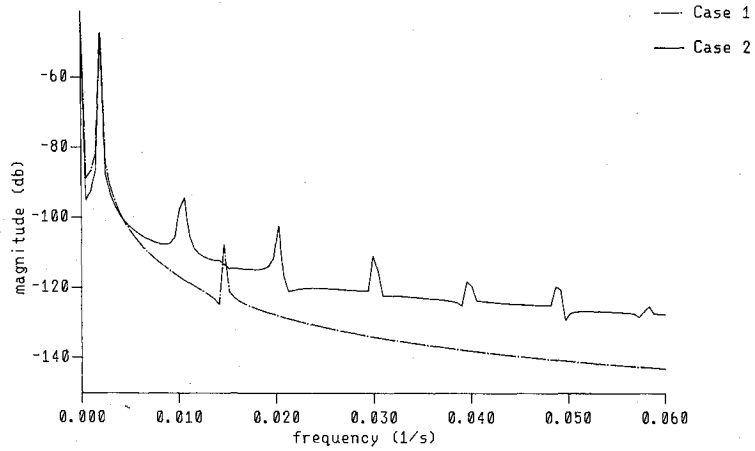

Fig. 7 Frequency spectrum of $[\tilde{y}(t)-\tilde{y}(t=0)]_l$ for $l_0=80$ km and $M=1000$ kg. Case 1: $C_d=C_D=0$; and Case 2: $C_d=C_D=2$.

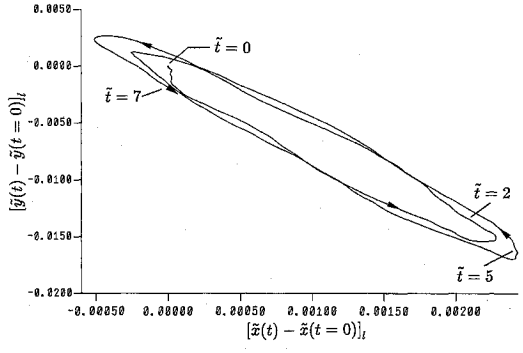

Fig. 8 Subsatellite trajectory ($l_0=95$ km, $M=1000$ kg).

of the physical quantities are expressed in dimensional units. The dimensional eigenvalues shown are those of the first (librating) mode and of the first predominantly longitudinal mode.

One should observe at this stage, from the data in Table 3, that the damping characteristics of the material of the tether reduce the value of the real part of the eigenvalues. As a consequence, neglecting the damping could lead to a wrong conclusion on the stability of an equilibrium configuration. This fact was already discussed with respect to the simple model in Ref. 8 and might prove to represent a way for passive control of the system. On the other hand, to ignore the damping leads to more conservative stability boundaries.

A few considerations on the calculated eigenvectors follow. If the shapes of the cable corresponding to the various modes are considered, the action of the aerodynamic forces does not sensibly change what can be observed in the case of no aerodynamic forces, as far as the general trend is concerned. In the absence of the atmosphere, the approximate analysis in Ref. 17 already showed the existence of an almost rigid pendular motion and of predominantly longitudinal and predominantly transverse motions. This is confirmed by the present numerical computations of the exact form of the linearized equations. However, the aerodynamic loads make the displacement components oscillate with a phase difference that is not $\pi/2$ anymore, although not very far from that value.

Table 4 shows, for the first three modes, the values of x_r and y_r, where the subscript r stands for eigenvector, at the free end of the cable. Two cases with no damping are compared, the first obtained when the aerodynamic forces are neglected, the second one when they are taken into account. The length of the cable and the mass of the subsatellite are 90 km and 1000 kg, respectively.

IV. Time Histories

To validate the results presented in the previous section and to extend the knowledge of the dynamic behavior of the system, solutions of the nonlinear differerential problem were sought. The adopted numerical method is based on a combination of the differential quadrature scheme as proposed in Ref. 16, and a rational Runge-Kutta integration procedure as reported and discussed in Ref. 18. As already stated, the spatial derivative at one of the N nodes, when the cable is divided into $(N-1)$ segments, are expressed as combinations of the values of the unknowns in a number L of adjacent nodes and, in so doing, the original system of partial differential equations is thus transformed into a finite set of ordinary differential equations, the time being the only independent variable. Expressing the spatial derivatives in an explicit form enables one to implement the boundary conditions immediately.

The second step in the solution procedure is the application of the rational Runge-Kutta method to the initial-value problem so obtained. Figure 7 provides some interesting results about the time history of a tether-subsatellite system that has been perturbed from its initial equilibrium state. In particular, the figure shows a comparison of the data from the Fourier analysis of the quantity $[\tilde{y}(t)-\tilde{y}(t=0)]_l$ for case 1, where the aerodynamic forces are neglected and for case 2, where these forces are taken into account. According to the linear stability analysis, case 1 corresponds to a stable equilibrium situation, while case 2 is relative to an unstable state. This is confirmed by the numerical results relative to the nonlinear problem. The atmospheric gradients and the aerodynamic forces act in such a way that the magnitude of the perturbations associated with a rather large number of frequencies is increased with respect to the case where these effects are not considered. Furthermore, the distance between the first two frequencies to which great values of the magnitude are associated sensibly decreases. The more realistic model for the system used here

confirms largely the conclusions of the simpler model in Ref. 8. A very simple explanation of the origin of the instability follows. During the motion caused by a perturbation of the initial equilibrium state, we have a pendular oscillation, elastic vibrations, and a periodic aerodynamic energy input which is forced by the Shuttle. The density gradient and the elasticity of the tether are such as to change continuously the frequency spectrum of the libration during the oscillation. It can happen that the frequency of the aerodynamic energy input comes within the spectrum of the libration, and resonance can occur.

Finally, Fig. 8 shows the trajectory of the subsatellite which follows a finite perturbation of an unstable equilibrium state. The corresponding shape of the tether does not significantly deviate from a straight line, at least for a few libration periods as in the case of a tether leaving from stable equilibrium conditions.[5]

V. Conclusions

It has been shown in this paper that the aerodynamic forces on the tether can have a great influence in most cases considered for practical applications, in particular as far as the stability of an equilibrium condition is concerned. It appears that future progress in the study of the dynamics of a tethered satellite will face increasingly hard problems as, for example, those connected with the stability of the system when the atmospheric density gradient and the shape of the geoid are both influencing a nonequatorial orbit of the Shuttle.

Acknowledgment

This work was partially supported by the Italian Ministry of Education.

References

[1]*Proceedings of the Workshop on Applications of Tethers in Space,* NASA CP-2364 and CP-2365, Marshall Space Flight Center, Huntsville, AL, 1983.

[2]*Proceedings of the Conference on Space Tethers for Science in the Space Station Era,* edited by L. Guerriero and I. Bekey, Società Italiana di Fisica, Bologna, Italy, 1988.

[3]*Proceedings of the Conference on Tethers in Space Towards Flight,* AIAA, NASA, ASI, ESA, San Francisco, CA, 1989.

[4]Boettcher, R. D., Koppenwallner, G., and Legge, H., "Aerodynamic Aspects of Tethered Satellite Design and Utilization," AIAA Paper 89-1562, May 1989.

[5]Misra, A. K., and Modi, V. J., "A Survey on the Dynamics and Control of Tethered Satellite Systems," *Advances in Astronautical Sciences,* Vol. 62, 1987, pp. 667–719.

[6]Beletskii, V. V., and Levin, E. M., "Dynamics of the Orbital Cable Systems," *Acta Astronautica,* Vol. 12, No. 5, 1985, pp. 285–291.

[7]Onoda, J., and Watanabe, N., "Tethered Subsatellite Swinging from Atmosphere Gradients," *Journal of Guidance, Control, and Dynamics,* Vol. 11, No. 5, 1988, pp. 477–479.

[8]de Matteis, G., and de Socio, L. M., "Influence of the Atmospheric Density Gradient on the Equilibrium of a Tether-Subsatellite System," *The European Journal of Mechanics, Pt. A/Solids,* Vol. 9, No. 3, 1990, pp. 1–16.

[9]Arnold, D. A., "Tether Tutorial," *Proceedings of the Conference on Space Tethers for Science in the Space Station Era,* edited by L. Guerriero and I. Bekey, Società Italiana di Fisica, Bologna, Italy, 1988, pp. 26–36.

[10]Colombo, G., Gaposchkin, E. M., Grossi, M. D., and Weiffenbach, G. C., "The Skyhook: a Shuttle-Born Tool for Low Orbital Altitude Research," *Meccanica,* Vol. 10, No. 1, 1975, pp. 3–20.

[11]Baker, W. P., Dunkin, J. A., Galaboff, Z. J., Johnston, K. D., Kissel, R. R., Rheinfurth, M. H., and Siebel, M. P. L., "Tethered Subsatellite Study," NASA TMX-73314, March 1976.

[12]Kalaghan, P. M., Arnold, D. A., Colombo, G., Grossi, M. D., Kirschener, L. R., and Orringer, O., "Study of the Dynamics of a Tethered Satellite System (Skyhook)," Final Rept., Contract NAS8-32199, March 1978.

[13]NOAA, NASA, USAF, *U.S. Standard Atmosphere,* Washington, DC, 1976.

[14]de Matteis, G., "Equilibrium Configurations of the Cable and Tethered Satellite System," *Proceedings of the 9th Congress AIMETA,* Centro Culturale Congressi, Bari, Italy, Oct. 1988, pp. 1–4.

[15]Bellman, R., and Roth, J., *Methods in Approximation,* D. Reidel, Boston, MA, 1986, Ch. 6, p. 125.

[16]Satofuka, N., "A New Explicit Method for the Numerical Solution of Parabolic Differential Equations," *Numerical Properties and Methodologies in Heat Transfer,* edited by T. M. Shih, Hemisphere, Washington, DC, 1983, pp. 97–108.

[17]Pasca, M., Pignataro, M., and Luongo, A., "Three-Dimensional Vibrations of Tethered Satellite Systems," *Journal of Guidance, Control, and Dynamics,* Vol. 14, No. 2, 1991, pp. 312–320.

[18]Paveri Fontana, S. L., and Srivastava, A., "Numerical Experiments on the Rational Runge-Kutta Method," *Computers and Mathematics with Applications,* Vol. 12, No. 12, 1986, pp. 1161–1170.